Meccanica
https://doi.org/10.1007/s11012-024-01833-y

Analysis of deformation in tensegrity structures with curved compressed members

Hannes Jahn · Valter Böhm · Lena Zentner

Received: 23 October 2023 / Accepted: 28 May 2024

Abstract Tensegrity structures are prestressed structures consisting of compressed members connected by prestressed tensioned members. Due to their properties, such as flexibility and lightness, mobile robots based on these structures are an attractive subject of research and are suitable for space applications. In this work, a mobile robot based on a tensegrity structure with two curved members connected by eight tensioned strings is analyzed in terms of deformation in the curved members. Further, the difference in locomotion trajectory between the undeformed and deformed structure after the prestress is analyzed. For that, the theory of large deflections of rod-like structures is used. To determine the relationship between acting forces and the deformation, the structure is optimized using minimization algorithms in Python. The results are validated by parameter studies in FEM. The analysis shows that the distance between the two curved members significantly influences the structure's locomotion. It can be said that the deformation of the components significantly influences the locomotion of tensegrity structures and should be considered when analyzing highly compliant structures.

Keywords Rolling locomotion · Mobile robot · Tensegrity structures · Deformation of compressed members · Finite element simulations

H. Jahn (✉) · L. Zentner
Department of Mechanical Engineering, Mechanics of Compliant Systems Group, P.O. Box 100565, 98693 Ilmenau, Germany
e-mail: hannes.jahn@tu-ilmenau.de

L. Zentner
e-mail: lena.zentner@tu-ilmenau.de

V. Böhm
Faculty of Mechanical Engineering, OTH Regensburg, P.O. Box 120327, 93025 Regensburg, Germany
e-mail: valter.boehm@oth-regensburg.de

1 Introduction

Tensegrity structures consist of compressed bars connected by strings in tension. As strings are stable but at the same time light and foldable, tensegrity structures have the potential to assume these properties [1]. And therefore have unique properties such as high flexibility, high compliance, adjustable stiffness and enormous strength to mass ratio [2]. Because of these advantages, the structures are, for instance, discussed for use in tensegrity robots for space applications. These robots can be divided into different categories [2], such as prismatic tensegrity robots [3–5], bio-inspired tensegrity robots [6–8] and spherical robots [9–12]. An example of a spherical robot is introduced by NASA as a tensegrity robot named SUPERBALL. Its structure is able to survive high-speed landings and locomotes to desired positions [12]. Due to the straight members of these conventional structures, their locomotion is produced by deformation

Published online: 12 June 2024

and tip-over sequences instead of actual rolling locomotion. Therefore, the authors in [13] introduced a specific class of spherical tensegrity structures with two curved members which is able to perform rolling locomotion [14, 15]. Two example mechanisms are shown in Fig. 1.

Previous research has shown that the application of curved members in tensegrity structures indicates their potential ability for use in rolling mobile robots. Two internal masses realized the actuation of the system. First, the two masses were shifted between the ends of the curved members on a straight line, which led to a restriction of the distance between the members [13]. Later the masses for the locomotion were shifted along the curved members [14]. Based on the results of that research, essential parameters, that influence the behavior of the system, are shown in [16]. In order to use such systems in space, an important parameter besides the volume is the mass of the system because even in times of reusable rockets, space-traveling is very expensive [17]. To reduce the mass of those structures, one possibility is to use smaller cross-sections of the curved members. This causes the problem that the curved members could be deformed due to the prestress of the structures. With the deformation of the system, the rolling motion should be influenced.

In this contribution, a detailed analysis of the deformation of the curved members of the structure is made and a parameter study is conducted to verify the analytical model. In Sect. 2 the structure and the forces acting in its members are described and analyzed. Upon this, an analytical model is set up in Sect. 3 where the equilibrium of the forces is used to describe the distance between the two bending members. The results of the analytical model are verified in a parameter study with a finite element model in Sect. 4 and a conclusion at the end.

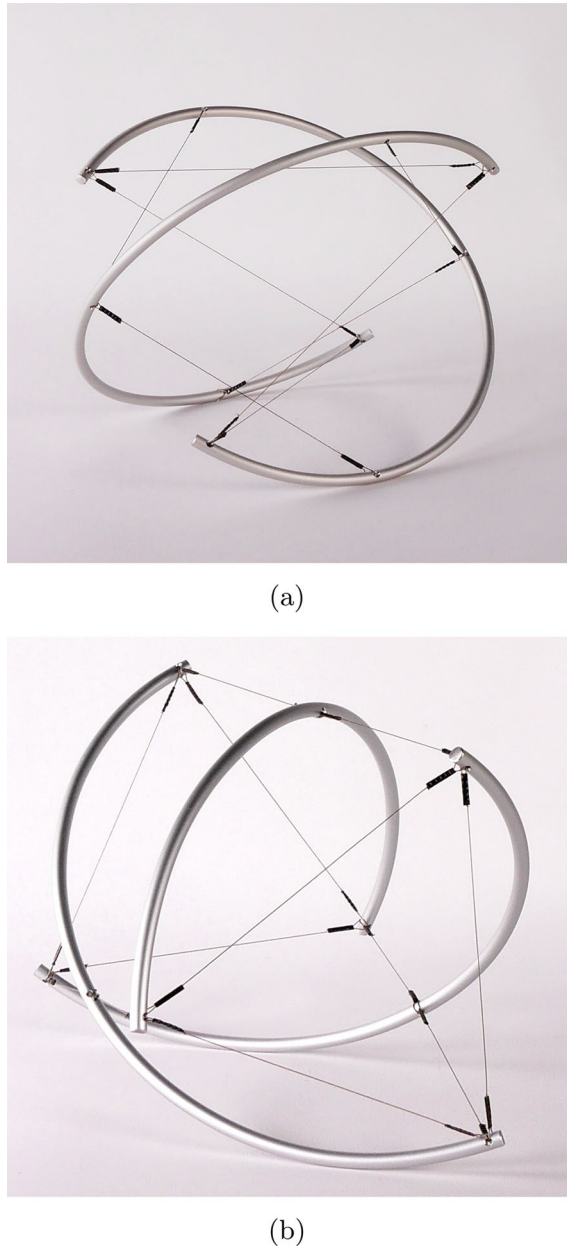

Fig. 1 Examples of tensegrity structures with curved members. (**a**) Structure with two curved members, connected by eight strings; (**b**) structure with three curved members connected by twelve strings

2 Description of the system and the forces

The considered tensegrity structure comprises two curved members, which are called bending members. It is based on the prototype B in [13]. It consists of two curved bending members, which are connected by eight tensioned strings at the ends of the bending members and in the middle of them, as shown in Fig. 2.

Therein, the thicker parts represent the curved bending members, which will be analyzed in terms of deformation. Dotted lines in blue are drawn between the ends of the curved bending members. The variable d indicates the distance between these lines. In

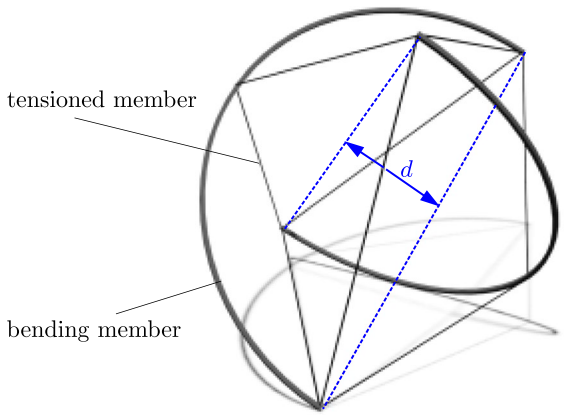

Fig. 2 The considered tensegrity structure on a plane with shadows

[16], this variable is highlighted as an important parameter in the locomotion behavior of the structure. The straight lines represent the tensioned members. Later, the tensioned members are modeled with variable lengths, as these only represent a force in the direction of the respective member. The figure also shows a shadow of the system to illustrate the contact points of the structure with the floor.

Tensegrity structures must be statically in equilibrium. If they were not, they would collapse. With the knowledge of the structure's appearance, an abstract model is shown in Fig. 3. Therein, all forces which act on one bending member are plotted. The forces in the middle of a bending member are defined as $F_{\mathrm{m}i}$ and the forces acting only at the ends are defined as $F_{\mathrm{e}i}$. These forces refer to the force's action on the strings. The index i is used to distinguish the forces of the strings. The absolute values of each of them are identical, assuming a precisely symmetrical structure.

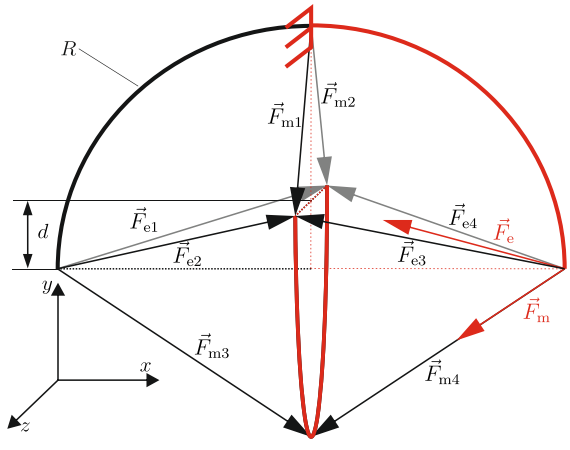

Fig. 3 Forces acting on one bending member in the tensegrity structure: (black) Whole structure with distance d between the centers of the bending members; (red) Part of the structure which is analyzed. (Color figure online)

Each force has the same impact on the opposite curved member. To get the structure in equilibrium, the inner forces have to be in equilibrium, as shown in Eq. (1).

$$\sum_{i=1}^{4} \vec{F}_{\mathrm{m}i} + \sum_{j=1}^{4} \vec{F}_{\mathrm{e}j} = \vec{0} \tag{1}$$

All forces $F_{\mathrm{m}i}$ and $F_{\mathrm{e}i}$ have different alignments in global coordinates. The symmetry of the structure leads to the fact that opposing forces dissolve each other. Only in y direction, the forces do remain. In Eq. (2), the force components in opposite directions are reduced.

$$\sum_{i=1}^{4} F_{\mathrm{m}i}\vec{e}_y + \sum_{i=1}^{4} F_{\mathrm{e}i}\vec{e}_y = \vec{0} \tag{2}$$

It follows from Eq. (2) that the forces in the y direction must be equal in opposite directions in order to keep the system in equilibrium.

Due to the symmetry of the structure, it is sufficient to only consider half of the whole structure for the analytical model, as can be seen in Fig. 3, shown in red. The half of the upper segment is modeled as a fixed end. At the other end, the beam is loaded by the forces F_{e} and F_{m}.

In Fig. 4, the locomotion of a structure with two curved members is shown three three-dimensional.

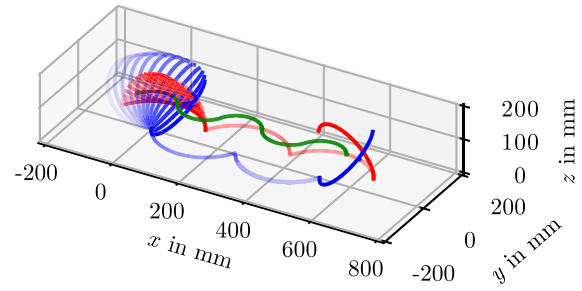

Fig. 4 Locomotion path of a structure to show how it toggles. One curved member is blue and one red. The green line represents the path of the center of gravity. (Color figure online)

It should be noted, that there is no influence of gravity. On the left side it can be seen how the structure turns around the point where the blue member has contact to the ground. The fading color shows where the locomotion starts. At the end of this first turn, the structure is performing the same turn around the contact point of the red member. In doing so, the contact lines of the members are shown on the ground ($z = 0$ mm). The green line represents the trajectory of the center of gravity of the structure. For this trajectory, only the line in the middle of the cross-section is used. In order of the small cross-section in comparison to the size of the structure, the differences should be neglectable.

With the knowledge of the locomotion behavior, the different locomotion pathes of that structure are shown in Fig. 5. The grey rectangles show the ratio d/R and it can be seen how the two members are arranged to each other. The structures themselves are undeformed, meaning that the curvature of the curved members is constant. The system moves from one member to the other in a tumbling motion. This means that while one member rolls along its curvature, the other is "standing" on its end-point, also called pivot point, as shown in the Fig. 5.

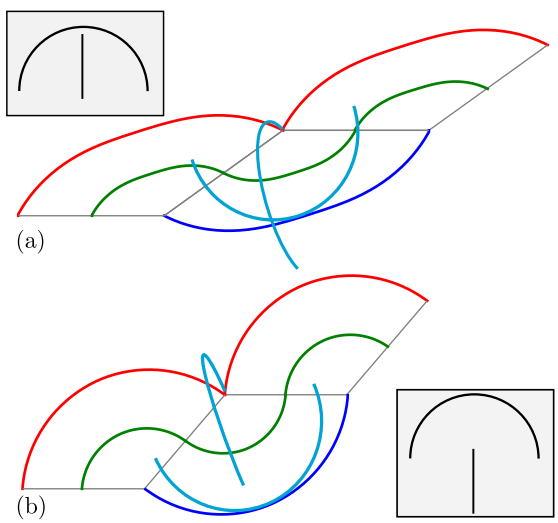

Fig. 5 Locomotion paths: (**a**) Path with $d/R = 0.9$; (**b**) Path with $d/R = 0.1$. Front view of both systems in grey boxes. Representation without tension members. Blue and red lines represent the contact points of each curved member. Green lines indicate the trajectory of the center point. (Color figure online)

In (a), it can be seen that with a higher d/R, more distance is covered by the structure. In (b), the traveling distance is lower, but the perpendicular movement of the structure's center rises.

3 Analytical description of the structure

An analytical description of the deformation of the curved flexural members is given by various models, such as Castigliano or elliptic integrals. An overview of the different models can be found in [18]. For the specific analysis of the locomotion of the structure, the whole nonlinear deformation along the beam axis is needed, and therefore the analysis of large deflections of rod-like structures is well suited. The analytical model to characterize the acting forces is based on the theory of large deflections of rod-like structures [19]. In literature, rod-like structures are defined as beams whose cross-sectional dimensions are at least ten times smaller than their length or curvature radii [19]. The structure in this work fulfills these requirements, so the theory is well suited for this application. To simplify the analysis, taking advantage of the symmetry of both bending members, only a quarter of the tensegrity structure is modeled.

The forces acting in the system are characterized to create an analytical model. For better understanding, they are shown in Fig. 6 for one counter-member. In this perspective, the second member is also cut in half on a slider in y-direction.

In Fig. 6 it can be seen that the force $\vec{F}_{\mathrm{e}}$ has components in each direction of the cartesian coordinate system. The force $\vec{F}_{\mathrm{m}}$, on the other hand, only acts in the direction of x and y. To determine the components of the forces, three angles, α, β and γ, are introduced. Due to the symmetry of the structure, the angle $\alpha = 225°$ stays the same all the time. Since the mechanism deforms simultaneously in every member, the angle between the members will always be the same. The other two angles are described by the coordinates from the endpoints of the two curved members. The formulas for determining them are given in Eq. (3).

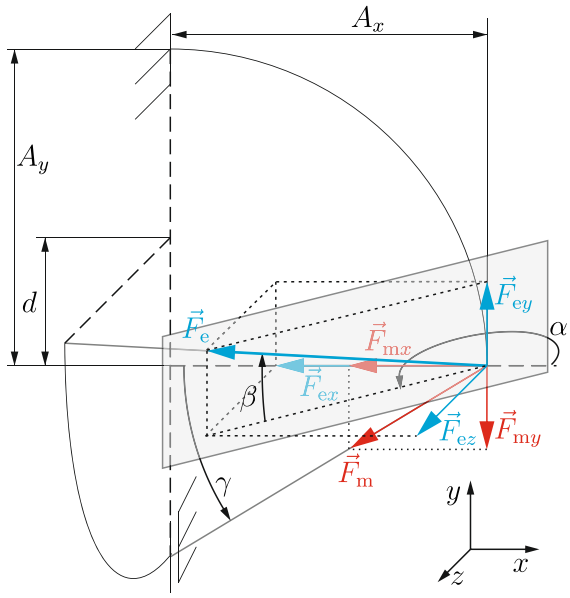

Fig. 6 Acting forces in one quarter of the tensegrity structure with curved members and introducing the three angles α, β and γ to determine the force-components. The slider at the bottom is a simplification of the symmetry

$$\begin{aligned}
\alpha &= \frac{5}{4}\pi, \\
\beta &= \arctan\frac{d}{\sqrt{A_x^2 + A_x^2}}, \\
\gamma &= \arctan\frac{A_y - d}{A_x}
\end{aligned} \tag{3}$$

With the angles from Eq. (3), the acting forces can be derived by using their components. So, the inner working forces are described by Eq. (4).

$$\begin{aligned}
F_{ex} &= \cos(\alpha)\cos(\beta)\cdot F_e \\
F_{ey} &= \sin(\beta)\cdot F_e \\
F_{ez} &= -\sin(\alpha)\cos(\beta)\cdot F_e \\
F_{mx} &= \cos(\pi+\gamma)\cdot F_m \\
F_{my} &= \sin(\pi+\gamma)\cdot F_m
\end{aligned} \tag{4}$$

For calculation purposes, the force F_{ez} is not relevant, as it is resolved by the symmetry of the structure.

3.1 Theory of large deflection of rod-like structures

For the used theory of large deflections of rod-like structures, the principle of ST. VENANT, BERNOULLI'S hypotheses and HOOKE'S law are assumed. The mathematical model is derived from the deflected state of a beam. That beam is described by its length, width, height, curvature and YOUNG'S modulus. The width and height result in a surface moment of inertia I_z for a rectangular cross-section.

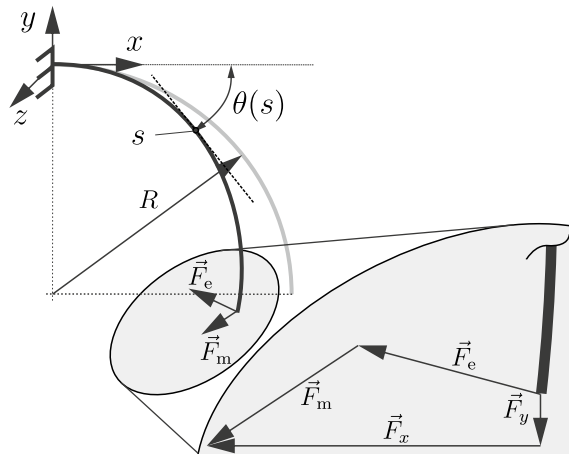

Fig. 7 Model of the analyzed quarter of the structure with important parameters for mathematical description with the theory of large deflections

The beam shown in Fig. 7 is fixed in the coordinate origin and loaded at the free end, which results in the deflected state due to consideration of large deflections. The beam-axis s is introduced in the deformed state. It describes a running parameter along the beam axis, along which the differential equation system can then be solved. A deflection angle θ results along the axis. From the before introduced forces F_m and F_e the forces F_x and F_y are the resulting directional forces in the cartesian coordinate system. The sum of the forces in directions x and y from Eq. (4) defines them in the respective directions. Due to the theory, the following system of differential equations is obtained:

$$\begin{aligned}
\frac{\mathrm{d}M_z}{\mathrm{d}s} &= F_x\sin\theta - F_y\cos\theta, \\
\frac{\mathrm{d}\theta}{\mathrm{d}s} &= \frac{M_z}{EI_z} + \kappa_0, \\
\frac{\mathrm{d}x}{\mathrm{d}s} &= \cos\theta, \\
\frac{\mathrm{d}y}{\mathrm{d}s} &= \sin\theta.
\end{aligned} \tag{5}$$

In these equations, M_z stands for the bending moment around the z-axis and κ_0 represents the curvature of the beam in the undeflected state, which is described by the reciprocal of the radius. To solve the system, boundary conditions are needed. They are shown in Eq. (6).

$$\begin{aligned} x(0) &= 0, \quad y(0) = 0, \\ \theta(0) &= 0, \quad M_z(0) = F_x A_y + F_y A_x. \end{aligned} \tag{6}$$

With these boundary conditions, an initial value problem is resolved. In this regard, the system is solved by using *Python*® with the help of the *scipy*-function *RK45*, which is a four-step RUNGE–KUTTA method for solving initial value problems. A flowchart of the solution process is shown in Fig. 8, marked in blue.

With that method, the deformation of one member can be found. In doing so, the directions of the forces change and with that, the values of them in Eq. (4) also change. In order to get the forces in equilibrium, it is possible to change the distance d. To solve the equilibrium in Eq. (1) of the structure another optimization tool is applied. With *scipy*'s function *minimize*, which is a root-finding method, the condition of Eq. (1) can be found with a specified accuracy. After each iteration, a new distance d is set, until a minimum, with a specified tolerance, is found.

The resulting forces are split up in their components in x and y direction with Eqs. (3) and (4).

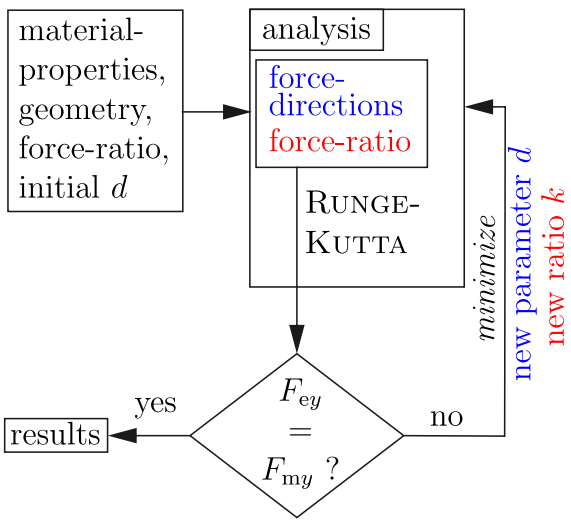

Fig. 8 Flowchart of the solution process to find the deformation of the structure and its distance d for given forces F_m and F_e (blue). Flowchart of the solution process for finding the force-relation to realize a specific distance d (red). (Color figure online)

3.2 Description of the FEM-model

The finite element method (FEM) is a numerical tool that enables approaching the solution of complex mechanical matters. In this context, the mechanical structure is discretized into a number of element bodies. The number of finite element bodies is defined in the model. In this work, the FEM model is set up in *Ansys Workbench 2021 R1* using the integrated *DesignModeler* to build the structure. The structure is constructed by a two-dimensional arc, corresponding to the neutral axis of a curved member, and a rectangular cross-section. In the initial state, the initial distance d between the curved members is equal to half of their radius. In *Mechanical*, the bodies are modeled as BEAM188 elements, whose are based on Timoshenko beam theory which includes shear-deformation effects, which at the same time are generally neglected for the used dimensions in this work. The forces are applied by using springs as connection elements. The initial tension of the springs is used to define the magnitude of the forces F_{ei} and F_{mi}. The analytical model uses constant forces. In the FEM model, the stiffnesses of the springs are set to a value close to zero in order to have minimal influence of additional elongation and therefore approach a constant force acting in these springs during the deformation of the structure. As boundary conditions, the model is fixed in the upper middle of the structure. With the use of the springs, the result represents the equilibrium of the inner forces of the system in the deflected state. *Probe-points* are used to compare the results of the displacements at the end of the fixed member in x and y direction. Displacements are indicated by the variables u with the corresponding directions in indices. A third *probe-point* in y-direction is used at one of the ends of the second member in y-direction to determine the final distance d, using the initial distance. The boundary condition and the *probe-points* are shown in Fig. 9.

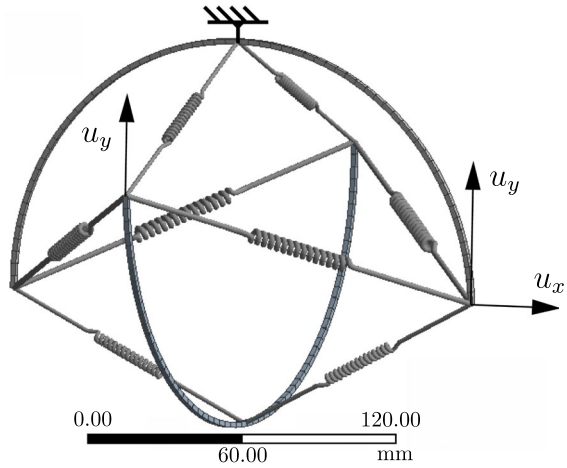

Fig. 9 FEM-Model with boundary condition and *probe-points* with the geometric dimensions used in the parameter study

4 Parameter studies with FEM and theory of large deflections of rod-like structures

In order to validate the built models, a parameter study is carried out. For that, both, FEM and analytical models, were loaded with a general force F, which is used to define a general load condition for the structure and reach a relationship between the forces at the ends and middle of the structure (F_e and F_m respectively). For that, a new parameter k is introduced. This parameter can take values between zero and one. The expressions for the forces F_e and F_m in terms of the parameter k and the general force F are given in Eq. (7).

$$F_\mathrm{e} = F \cdot k \qquad F_\mathrm{m} = F(1-k) \tag{7}$$

As the parameter k varies from 0 to 1, the values for F_e and F_m varies from 0 to F, as shown in Eq. (7). The geometric dimensions used in the parameter study are given in Table 1. The strucures YOUNGS's modulus is $E = 72,000\,\mathrm{MPa}$, representing an aluminium.

The first part of the study analyzes the relation between the ratio k and the distance d. As it is shown in Fig. 10, it is a complex relation between these parameters and cannot be simplified as a linear equation, leading to the conclusion, that the problem's solution is also not trivial. In Fig. 10a for $k = 0.05$ the results for the distance d are out of the contour, which leads to the idea of numerical errors because

Table 1 Geometric dimensions of the analyzed structure with initial distance d

Geometrical dimension	Magnitude
Width	$w = 2\,\mathrm{mm}$
Height	$h = 2\,\mathrm{mm}$
Radius	$R = 100\,\mathrm{mm}$
Initial distance	$d = 50\,\mathrm{mm}$

the rest of the curves are continuous similar to the FEM results.

The second part of the parameter study is conducted to validate the analytical model and the results are presented in Fig. 11. The points in the diagrams represent the parameters investigated; the lines are only drawn for clarity. The graph in Fig. 11a shows the deviation, of the distance d from the analytical

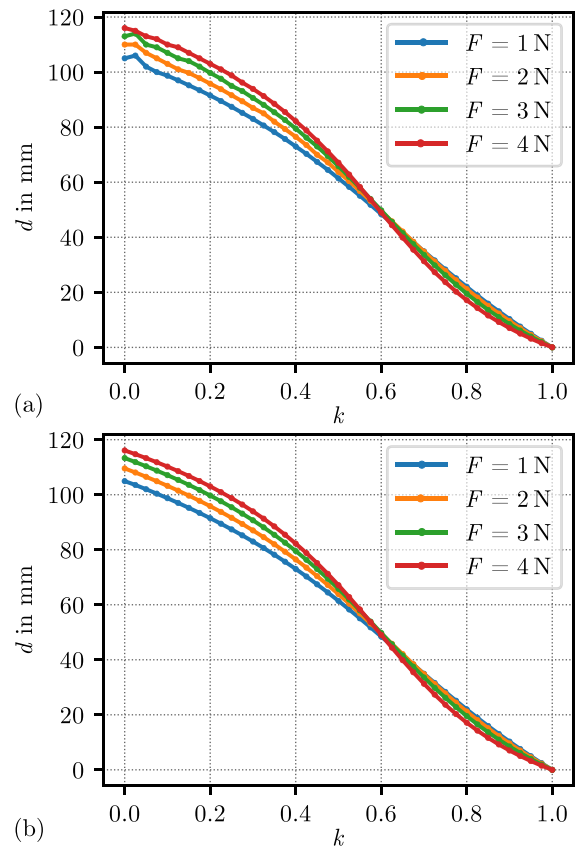

Fig. 10 Parameter study with variation of the parameter $0 \leq k \leq 1$ with general forces F from 1 N to 4 N: Distance d over k; (**a**) Analytical model; (**b**) FEM simulation

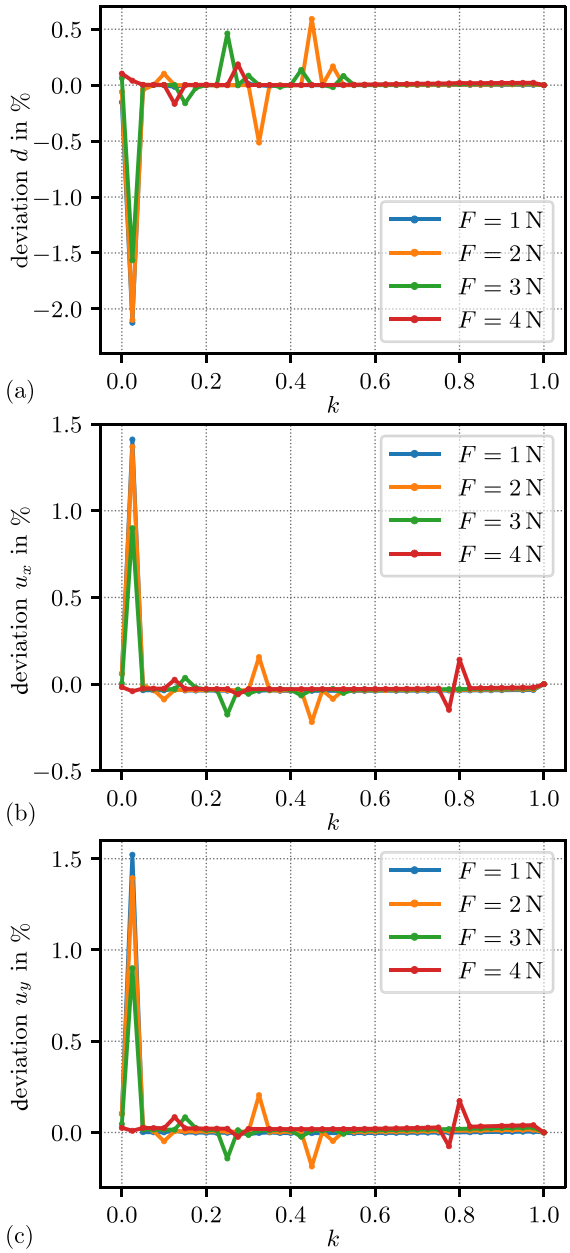

Fig. 11 Parameter study with variation of the ratio $0 \leq k \leq 1$ with general forces from 1 N to 4 N: (**a**) Deviation of the distance d from the analytical model to the FEM-model over k; (**b**) Deviation of the endpoints of the analytical model to the endpoints of the FEM-model in x-direction; **(c)** Deviation of the endpoints of the analytical model to the endpoints of the FEM-model in y-direction

model to the FEM-model, over k. At a few points, the graphs show some peaks, which can be interpreted as numerical errors in the analytical solution, similar

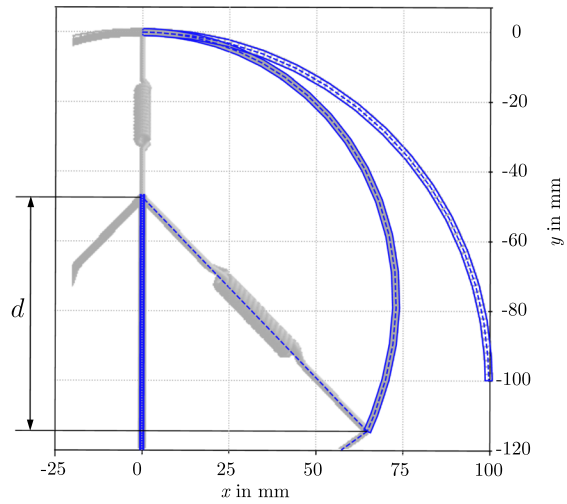

Fig. 12 Overlay of the FEM-calculated deformation in grey with a plot of the analytical calculation in blue. Parameter d in deflected state. (Color figure online)

to the before mentioned irregularity in Fig. 10, and therefore, they can be neglected. Overall, the analytical model with a maximal deviation of around 0.1% is accurate compared to FEM. The parameter studies proved that the endpoints of the single rods are also similar to the FEM-model. The displacements u_x and u_y are also only diverting about 0.1%, regarding the few peaks as numerical errors, as can be seen in Fig. 11b and c. The deviations of the displacement u_x and u_y become higher with higher acting forces but are nevertheless small. In this comparison, only the endpoints are regarded. Besides the endpoints, it is important to compare if the actual beam axis is also aligning between the models.

Figure 12 shows an overlay of the deformed and undeformed structure from the FEM- and the analytical model to represent the acquired results along the beam axis. Therein the three-dimensional grey construct of the structure is the FEM solution and the blue overlay on the plot is the solution from the analytical model. Both figures are scaled to the same dimensions and are aligned. This shows representative the small deviations between both models, it can also be seen, that the whole axis of the bending member aligns. This is relevant for later calculating the rolling locomotion in the deformed state. With the shown distance d it can also be seen, how the deformation influences that distance. With that

parameter study, the analytical model is validated using the theory of large deflections of rod-like structures for tensegrity structures.

In Fig. 13 a graphical explanation of the calculation of the rolling paths is shown. Therefore the calculated quarter of the beam axis is mirrored to get information of the whole bending member. After that, the second bending member is arranged with the distance d. In Fig. 13a the structure is shown at the beginning of one rolling iteration. With the grey surface, the rolling contour is highlighted. Along that surface, two new variables are introduced. First the distance a and second the angle δ. a is calculated with the geometric information of the two bending members in the cartesian space with Eq. (8).

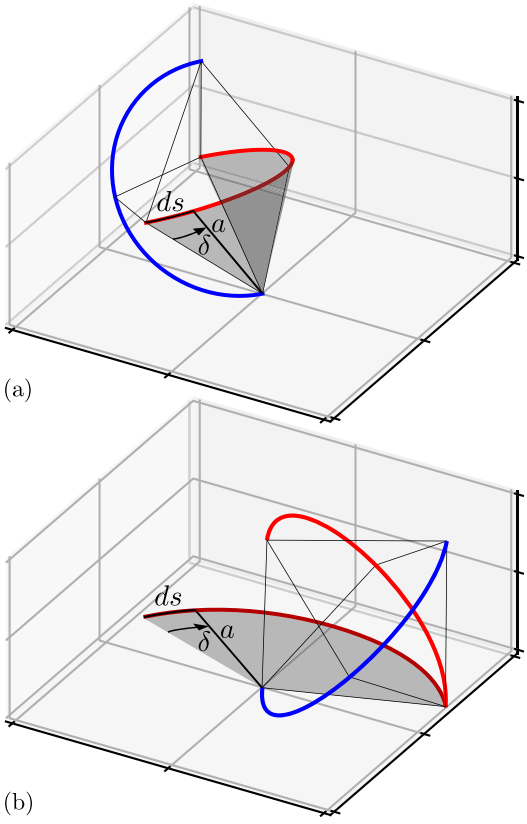

Fig. 13 Rolling behavior of the tensegrity structure: (**a**) Structure with the rolling path and the curved grey face which then is shown after rolling in (**b**). (Color figure online)

$$a(s) = \Big(\big(x_1(s=0) - x_2(s)\big)^2 + \big(y_1(s=0) - y_2(s)\big)^2 + \big(z_1(s=0) - z_2(s)\big)^2 \Big)^{\frac{1}{2}} \tag{8}$$

The indices 1 and 2 distinguish the respective members. With a and ds, the angle δ is calculated with:

$$\delta(s) = \arcsin \frac{\mathrm{d}s}{a(s)}. \tag{9}$$

So, the structure's motion path can be calculated with the angle δ and the distance a, similar to Fig. 13b in the plane $(z = 0)$. This procedure is repeated for the next curves in order to represent a complete locomotion.

As mentioned before, the deformed structure has a different locomotion behavior than the undeformed structure due to the varying curvature of the bending members. This is represented visually in Fig. 14, where the locomotion paths of the structure for different d/R are shown in the deformed and undeformed states. The motion paths for the structure, with a ratio $d/R = 0.9$, in the undeformed and deformed states, are shown in Fig. 14a and b, respectively. It can be seen that the motion of the same structure changes significantly under deformation, which can be advantageous for different applications. A noticeable difference can also be seen for a structure with $d/R = 0.1$ in Fig. 14c and d.

To produce the locomotion paths of the different structures, the distance of the point to the other curved member is used.

After the successful validation of the analytical model with the help of FEM-analyzes, and the knowledge that the distance d and the deformation significantly impact the locomotion behavior of the structure, a new model is set up, where it is possible to specify a certain distance d. It is similar to the previous solution process. The optimization is therefore also shown in Fig. 8, marked by the red colors.

The main difference to the first analytical models is that the parameter d is the goal of this optimization. To achieve a special distance d, the *minimize*-function gives a new ratio k after each iteration. That ratio k influences the forces as shown in Eq. (7), until the forces in y-direction are equal for that specific distance d. It is possible to set the right forces on the

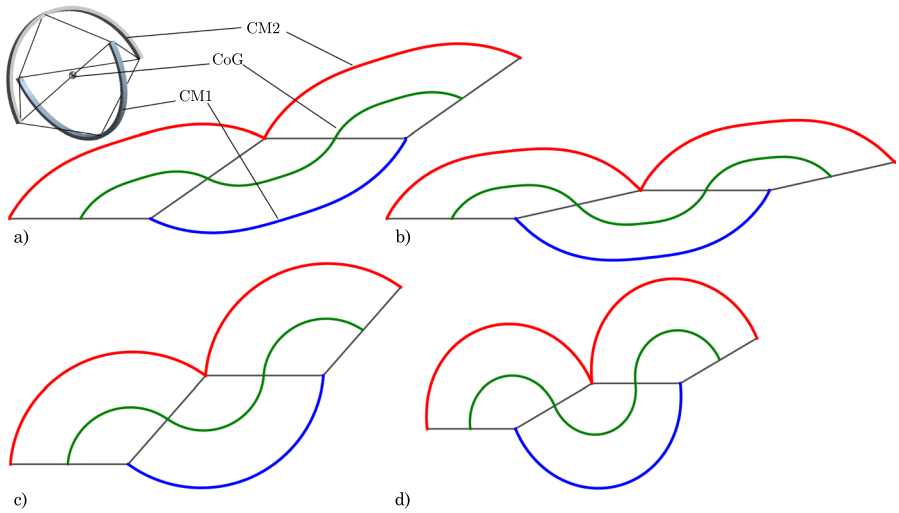

Fig. 14 Locomotion of initial and deformed structure: upper and lower arcs (red and blue) representing contact lines of curved member 1 and 2 (CM1, CM2); middle line (green) represents center of gravity (CoG)-track. (**a**) Initial structure with $d/R = 0.9$; (**b**) Deformed structure with $d/R = 0.9$; (**c**) Initial structure with $d/R = 0.1$; (**d**) Deformed structure with $d/R = 0.1$. (Color figure online)

Table 2 Geometric dimensions of the structure for the method's application with calculated force to feed the FEM-model

Geometrical dimension	Magnitude
Width	$w = 6\,\text{mm}$
Height	$h = 4\,\text{mm}$
Radius	$R = 85\,\text{mm}$
YOUNGS'S modulus	$E = 72,000\,\text{MPa}$
General force	$F = 10\,\text{N}$
Calculated force	$F_\text{e} = 4.04\,\text{N}$
Calculated force	$F_\text{m} = 5.96\,\text{N}$

Table 3 Calculated displacements from the analytical model and the FEM-model with forces from the analytical model

	Analytical (mm)	FEM (mm)	Deviation (‰)
u_x	−2.062	−2.063	0.605
u_y	−1.260	−1.260	0.043
d	59.5	59.5	0.002

With the relative deviations from the FEM-model

tensioned members to influence the distance d and the bending members in their shape to influence the system's locomotion behavior.

As an application, it is conceivable to adjust the forces in the system for a given trajectory so that a desired locomotion is achieved.

5 Application of the developed method

Following, an example is investigated using the developed method. The results from the above-presented optimization are the forces F_m and F_e, calculated from a given general force F and the distance d. In Order to verify the developed method, a given structure with the geometric dimensions presented in Table 2 oriented to the structure from [14] is analyzed.

In [14] the authors analyze a structure with a ratio $d/R = 0.7$ which leads to a desired distance $d = 59.5$ mm. For the application of the method, the cross-sectional dimensions are estimated. The goal of the method is to predict the forces in the system to get the given distance. To calculate the ratio of the forces, the describing parameters, including a general force, are written in the script. The calculated forces are given to the FEM-model, to validate the deformation and the resulting distance. With the *probe-points* (see Sect. 4), the distance is evaluated and compared with the desired number. The calculated forces and displacements are given in Table 3.

The differences in the deformation and the distance between the analytical and FEM solutions are minimal, with a deviation of less than one per mille. With this application, it is shown how reliable the calculation works.

6 Conclusions

With this contribution, the authors presented an analytical method to describe the elastic behavior of

tensegrity structures with curved bending members. The analytical calculations in this paper are based on the theory of large deformations of rod-like structures. It was shown that there is an analytical possibility to adjust the parameter d by applying different forces to the tensile strings in the system. The analytical results generated were successfully validated in a parameter study using FEM. The calculations can be easily applied and are very time-saving compared to FEM simulations. In addition, the influence of the deformation of the bending members on the system's locomotion behavior was presented for different parameters d. The deformation should not be neglected when considering highly compliant systems, because it has a great influence on the locomotion behavior. Adding another optimization goal made it possible to generate a specified distance d using force relations. This feature allows setting forces between the two curved members to achieve specific locomotion behavior. It has been tested and presented with a validation in FEM. The results from analytical and FEM models exhibit negligible differences between them, demonstrating accurate estimations. In addition, based on these investigations, it is conceivable to actively regulate and adjust the parameter d and therefore the deformation during locomotion. Subsequent studies could investigate the extent to which gravitation influences movement behavior. However, this would have to include further considerations, as the structure's symmetry would no longer be guaranteed. In addition, the forces in the tension members considered in this work could be applied to actual tensioned members, in which tension is then considered.

Acknowledgements The authors would like to gratefully acknowledge the support of the German Research Foundation (DFG) within the SPP2100 under grant numbers (ZE 714/14-2) and (BO 4114/3-2).

Funding Open Access funding enabled and organized by Projekt DEAL.

Declarations

Conflict of interest The authors declare that they have no conflict of interest.

References

1. Skelton RE, Adhikari R, Pinaud JP et al (2001) An introduction to the mechanics of tensegrity structures. In: Proceedings of the 40th IEEE conference on decision and control (Cat. No.01CH37228). IEEE, pp 4254–4259. https://doi.org/10.1109/CDC.2001.980861
2. Liu Y, Bi Q, Yue X et al (2022) A review on tensegrity structures-based robots. Mech Mach Theory 168:104571. https://doi.org/10.1016/j.mechmachtheory.2021.104571
3. Cefalo M, Mirats-Tur JM (2011) A comprehensive dynamic model for class-1 tensegrity systems based on quaternions. Int J Solids Struct 48(5):785–802. https://doi.org/10.1016/j.ijsolstr.2010.11.015
4. Paul C, Valero-Cuevas FJ, Lipson H (2006) Design and control of tensegrity robots for locomotion. IEEE Trans Robot 22(5):944–957. https://doi.org/10.1109/TRO.2006.878980
5. Vasquez RE, Correa JC (2007) Kinematics, dynamics and control of a planar 3-DOF tensegrity robot manipulator. In: Volume 8: 31st mechanisms and robotics conference, Parts A and B. ASMEDC, pp 855–866. https://doi.org/10.1115/DETC2007-34975
6. Jung E, Ly V, Cessna N et al (2018) Bio-inspired tensegrity flexural joints. In: Lynch K (ed) 2018 IEEE international conference on robotics and automation (ICRA). IEEE, Piscataway, NJ, pp 5561–5566. https://doi.org/10.1109/ICRA.2018.8461027
7. Lessard S, Castro D, Asper W et al (2016) A bio-inspired tensegrity manipulator with multi-DOF, structurally compliant joints. In: 2016 IEEE/RSJ international conference on intelligent robots and systems (IROS). IEEE, pp 5515–5520. https://doi.org/10.1109/IROS.2016.7759811
8. Shintake J, Zappetti D, Peter T et al (2020) Bio-inspired tensegrity fish robot. In: 2020 IEEE international conference on robotics and automation (ICRA). IEEE, Piscataway, NJ, pp 2887–2892. https://doi.org/10.1109/ICRA40945.2020.9196675
9. Chen LH, Cera B, Zhu EL et al (2017a) Inclined surface locomotion strategies for spherical tensegrity robots. In: 2017 IEEE/RSJ international conference on intelligent robots and systems (IROS). IEEE, pp 4976–4981. https://doi.org/10.1109/IROS.2017.8206380
10. Chen LH, Kim K, Tang E et al (2017) Soft spherical tensegrity robot design using rod-centered actuation and control. J Mech Robot 9(2):025001. https://doi.org/10.1115/1.4036014

11. Kim K, Chen LH, Cera B et al (2016) Hopping and rolling locomotion with spherical tensegrity robots. In: 2016 IEEE/RSJ international conference on intelligent robots and systems (IROS). IEEE, pp 4369–4376. https://doi.org/10.1109/IROS.2016.7759643
12. Vespignani M, Friesen JM, SunSpiral V et al (2018) Design of superball v2, a compliant tensegrity robot for absorbing large impacts. In: 2018 IEEE/RSJ international conference on intelligent robots and systems (IROS). IEEE, pp 2865–2871. https://doi.org/10.1109/IROS.2018.8594374
13. Böhm V, Jentzsch A, Kaufhold T, et al (2011) An approach to compliant locomotion systems based on tensegrity structures. In: International Scientific Colloquium Technische Universität Ilmenau, Faculty of Mechanical Engineering, 56 (Ilmenau) : 20110912-16 56
14. Kaufhold T, Schale F, Bohm V et al (2017) Indoor locomotion experiments of a spherical mobile robot based on a tensegrity structure with curved compressed members. In: 2017 IEEE international conference on advanced intelligent mechatronics (AIM). IEEE, pp 523–528. https://doi.org/10.1109/AIM.2017.8014070
15. Schorr P, Li ERC, Kaufhold T et al (2021) Kinematic analysis of a rolling tensegrity structure with spatially curved members. Meccanica 56(4):953–961. https://doi.org/10.1007/s11012-020-01199-x
16. Böhm V, Kaufhold T, Zeidis I et al (2017) Dynamic analysis of a spherical mobile robot based on a tensegrity structure with two curved compressed members. Arch Appl Mech 87(5):853–864. https://doi.org/10.1007/s00419-016-1183-z
17. Harris TM, Landis AE (2019) Space sustainability engineering: quantitative tools and methods for space applications. In: 2019 IEEE aerospace conference. IEEE, pp 1–6. https://doi.org/10.1109/AERO.2019.8741939
18. Ghuku S, Saha KN (2017) A review on stress and deformation analysis of curved beams under large deflection. Int J Eng Technol 11:13–39. https://doi.org/10.18052/www.scipress.com/IJET.11.13
19. Zentner L, Linß S (2019) Compliant systems: mechanics of elastically deformable mechanisms, actuators and sensors. De Gruyter, Berlin and Boston. https://doi.org/10.1515/9783110479744